Electronic Supplementary Material (ESI) for Journal of Materials Chemistry C.

Supporting Information For

Constructing moisture-stable hybrid lead iodine semiconductors based on hydrogen-bond avoiding and dual-iodine strategies

Guang-Ning Liu,*[,a] Ruo-Yu Zhao,[a] Rang-Dong Xu,[a] Qisheng Liu,[a] Bo Xu,[a] Yang-Yang Wang,[a] Qian Wu,[a] Jun-Nuan Wang,[a] Yong Nie,[a] and Cuncheng Li*[,a]

[a]*School of Chemistry and Chemical Engineering, University of Jinan, Jinan Shandong 250022, PR China*

Contents

S 1.1 Materials and characterization

All reagents were purchased commercially and used without further purification. Elemental analyses of C, H, and N were performed on an Elementar Vario EL III microanalyzer. Powder X-ray diffraction (PXRD) patterns were recorded on Bruker D8 Focus diffractometer using Cu $K\alpha$ radiation. A Perkin-Elmer Diamond thermogravimetric analyzer was used to obtain thermogravimetric analyses (TGA) curves in N_2 with a flow rate of 20 $mL \cdot min^{-1}$ and a ramp rate of 10 $°C \cdot min^{-1}$ in the temperature range 40–900 °C. An empty Al_2O_3 crucible was used as the reference. The FT-IR spectra were obtained on a Perkin-Elmer spectrophotometer using KBr disk in the range 4000–400 cm^{-1}. Optical diffuse reflectance spectra were measured at room temperature with a Shimadzu UV-3101 PC UV-vis spectrophotometer. The instrument was equipped with an integrating sphere and controlled with a personal computer. The samples were ground into fine powder and pressed onto a thin glass slide holder. A $BaSO_4$ plate was used as a standard (100% reflectance). The absorption spectra were calculated from reflectance spectrum using the Kubelka-Munk function:[1] $\alpha/S = (1-R)^2/2R$ where α is the absorption coefficient, S is the scattering coefficient (which is practically wavelength independent when the particle size is larger than 5 μm), and R is the reflectance.

S 1.2 Computational details

The X-ray crystallographic data of the four hybrids was used to calculate its electronic structure. The calculations of density of states (DOS) were carried out using density functional theory (DFT) with one of the three nonlocal gradient-corrected exchange-correlation functionals (GGA-PBE) and performed with the CASTEP code,[2] which uses a plane wave basis set for the valence electrons and norm-conserving pseudopotential for the core electrons.[3] Pseudo-atomic calculations were performed for Pb $5d^{10}6s^26p^2$, Cu $3d^{10}4s^1$, Mn $3d^54s^2$, I $5s^25p^5$, Cl $3s^23p^5$, C, $2s^22p^2$, N $2s^22p^3$ and H $1s^1$. The parameters used in the calculations and convergence criteria were set by the default values of the CASTEP code.[2]

S 1.3 Single-crystal structure determination

The intensity data sets were collected on a Agilent Xcalibur, Eos, Gemini CCD diffractometer equipped with a graphite-monochromated Mo Kα radiation (λ = 0.71073 Å) at 293 K. The data sets were reduced by the CrysAlisPro[4] program. An empirical absorption correction using spherical harmonics was implemented in SCALE3 ABSPACK scaling algorithm. The structures were solved by direct methods using the Siemens SHELXL package of crystallographic software.[5] Difference Fourier maps were created on the basis of these atomic positions to yield the other non-hydrogen atoms. The structures were refined using a full-matrix least-squares refinement on F^2. All non-hydrogen atoms were refined anisotropically. The hydrogen atoms of were located at geometrically calculated positions and refined as riding on their parent atoms with fixed isotropic displacement parameters [$U_{iso}(H) = 1.2U_{eq}(C, N)$]. In the binuclear metal complex cations of **bi-MnPhen-Pb_2I_6**, both the I and Cl act as bridging atoms at two disordered sites with occupancies of 0.35 and 0.65, respectively. Crystallographic data and structural refinements for four hybrids are summarized in Table S1. Important bond lengths and angles are listed in Table S8.

The phase purities of four hybrids for physical property measurements were confirmed by PXRD studies. The experimental PXRD patterns coincide fairly well with the simulated patterns from the single-crystal structures, which reveal the phase purity of the bulk crystalline materials.

S2 Synthetic considerations

In this work, alkylated Bpy cations, mononuclear and binuclear metal complex cations were all formed in situ to direct the formation of hybrid iodoplumbates. The formation of alkylated $(Et_2Bpy)^{2+}$ cations involve the facile in situ N-alkylation reactions, where the ethyl group was formed from the cleavage of C–O bonds of organic alcohols. The N donor was positive charged after the reaction. The reaction temperature plays an important role on the formation of hybrids **EtBpy-Pb_3I_8** and **EtBpy-Pb_2I_6**, which were obtained from the same reactant, but with different inorganic iodoplumate species. During the synthesis of **CuIBpy-Pb_2I_6**, the attempt to get its Phen-analogue using Phen instead of Bpy was fruitless. Further experiments indicate that the absence of NH_4SCN in the synthesis of **bi-MnPhen-Pb_2I_6** will lead the yield greatly decreased. Correspondingly, the attempts of using Bpy instead of Phen to get the Bpy analogue of **bi-MnPhen-Pb_2I_6** were unsuccessful. The reaction temperatures

described in the synthesis detail are optimized, and large deviations of these temperatures will not generate the proposed products.

Table S1 Crystal and Structure Refinement Data.

	EtBpy-Pb_3I_8	**EtBpy-Pb_2I_6**	**CuIBpy-Pb_2I_6**	**bi-MnPhen-Pb_2I_6**
Formula	$C_{14}H_{18}N_2I_8Pb_3$	$C_{14}H_{18}I_6N_2Pb_2$	$C_{40}H_{32}Cu_2I_8N_8Pb_2$	$C_{48}H_{32}Cl_{1.29}I_{6.71}Mn_2N_8Pb_2$
M_r (g mol^{-1})	1851.07	\1390.08	2181.39	2142.30
Crystal system	Monoclinic	\Orthorhombic	Monoclinic	Triclinic
Space group	$P2_1/n$	\$P$bca	$P2_1/c$	P–1
ρ_{calcd} [g cm^{-3}]	3.762	3.324	2.648	2.514
a [Å]	7.8325(3)	18.1901(13)	17.9449(10)	12.0083(6)
b [Å]	22.8994(6)	15.8183(10)	19.4236(11)	15.9672(8)
c [Å]	18.3031(8)	19.3077(15)	7.8786(3)	16.8500(9)
α [°]	90	90	90	71.256(5)
β [°]	94.994(4)	90	94.945(4)	77.764(4)
γ [°]	90	90	90	68.460(5)
V [Å^3]	3270.4(2)	5555.5(7)	2735.9(2)	2829.6(3)
Z	4	8	2	2
T [K]	293(2)	293(2)	293(2)	293(2)
F(000)	3144	4784	1948	1935
θ range [°]	3.28–25.50	3.00–25.50	3.11–25.50	3.25–25.50
Measured reflections	18809	22082	16055	43227
Independent reflections (R_{int})	6085 (0.0560)	5154 (0.0647)	5081 (0.0494)	10505 (0.0372)
Data/params/restraints	4665/245/0	3310/219/0	3563/271/36	8771/623/0
R_1[a], wR_2[b] [$I>2\sigma(I)$]	0.0405, 0.0808	0.0392, 0.0637	0.0434, 0.0828	0.0371, 0.0859
Goodness of fit	1.031	0.996	1.056	1.075

$\Delta\rho_{max}$ and $\Delta\rho_{min}$ [e Å^{-3}]	2.181, –1.606	1.326, –1.627	1.315, –1.181	1.545, –1.043

$^{a}R_1 = \sum||F_o|-|F_c||/\sum|F_o|$, $^{b}wR_2 = \{\sum w[(F_o)^2-(F_c)^2]^2/\sum w[(F_o)^2]^2\}^{1/2}$

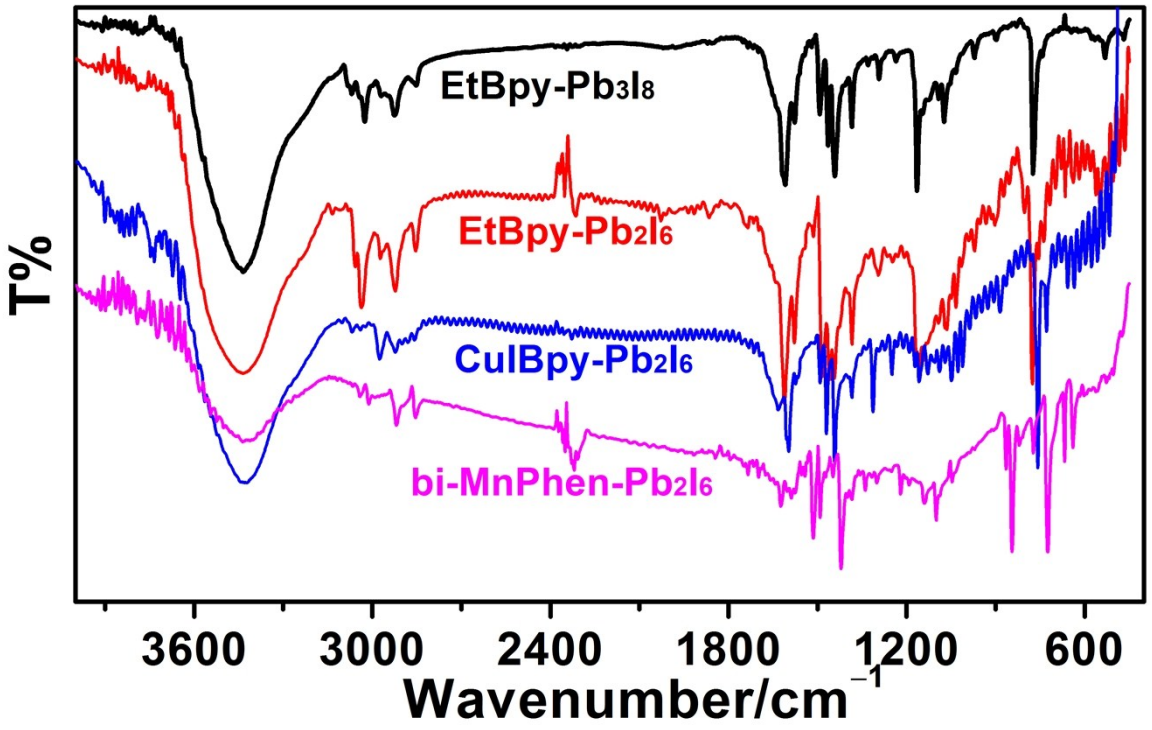

Fig. S1 IR spectra of the four lead iodine hybrids.

Table S2 IR Spectral Data (KBr pellet, cm^{-1}).

EtBpy-Pb_3I_8	3435(vs), 3026(w), 2925(w), 1609(s), 1577(m), 1442(m), 1385(m), 1165(s), 1074(m), 774(s), 528(w).
EtBpy-Pb_2I_6	3434(s), 3037(m), 2922(w), 2854(vw), 1612(vs), 1576(m), 1459(m), 1385(m), 1158(m), 776(s), 549(w).
CuIBpy-Pb_2I_6	3428(vs), 3073(vw), 2977(w), 2926(vw), 1595(m), 1473(m), 1438(m), 1386(vw), 1313(m), 1248(m), 1157(vw), 753(vs).
bi-MnPhen-Pb_2I_6	3424(vs), 3025(s), 2852(vw), 1595(m), 1568(m), 1499(m), 1443(m), 1382(m), 1356(s), 1209(w), 1117(w), 1065(vw), 1027(s), 979(s), 935(s), 880(w), 753(vs).

S3 IR analysis

For the four lead iodine hybrids, the relatively weak bands in the region of 3000–3100 cm^{-1} correspond to the C–H vibrations of the aromatic ring hydrogen atoms, ν(=C–H). The bands of ring vibrations of the conjugated ligand (ν(C=C) and ν(C=N)) are observed at 1640–1400 cm^{-1}, suggesting the existence of conjugated organic cations. The broad bands in the range 3500–3300 cm^{-1} for all are assigned to the stretching of trace water since the measurements were conducted in air. The above results are all in agreement with the single crystal X-ray diffraction studies.

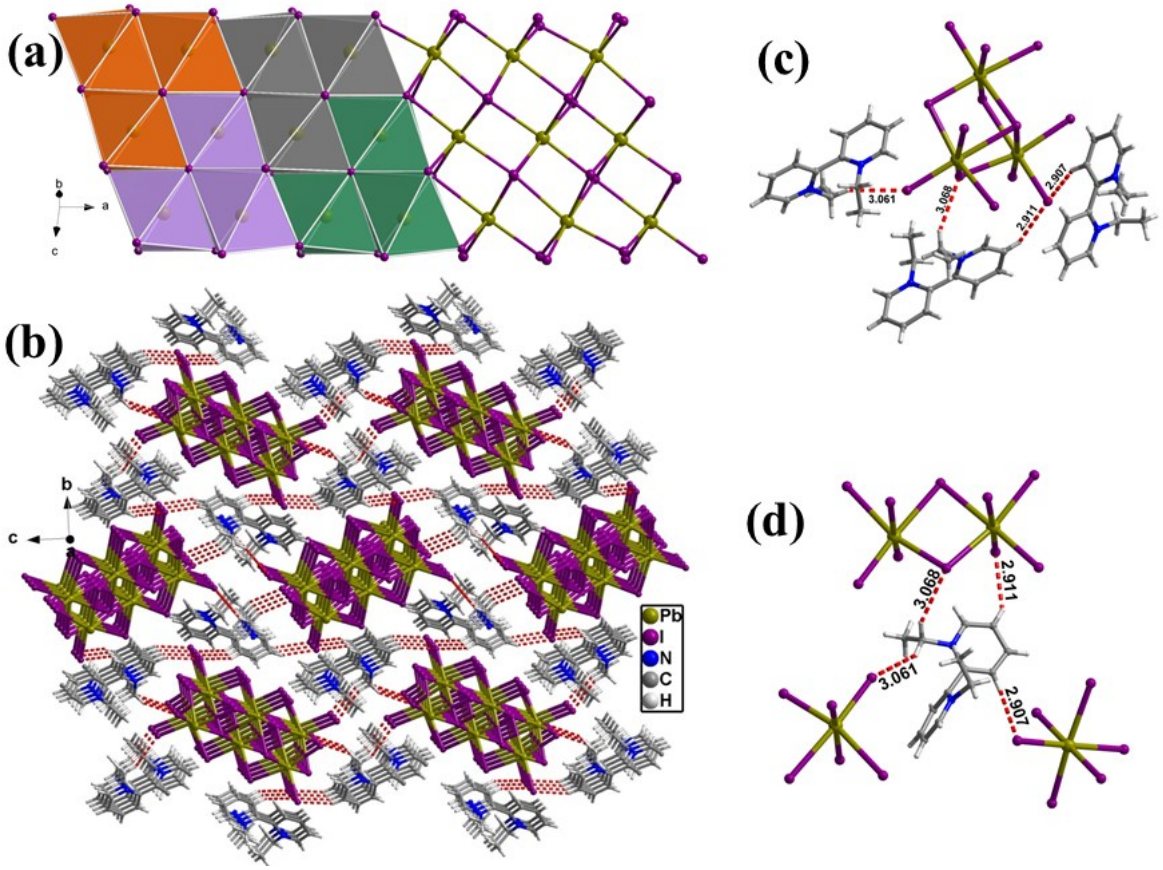

Fig. S2 (a) Showing the stacking of the trinuclear (Pb_3I_{14}) units to form the zigzag-like $(Pb_3I_8)^{2-}$ chain. (b) The 3-D supramolecular framework of **EtBpy-Pb_3I_8**. (c, d) A close view of the C–H···I hydrogen bond (red dashed lines) around a inorganic $(Pb_3I_8)^{2-}$ chain and a $(Et_2$2,2'-bipy$)^{2+}$ cation, respectively.

Table S3 Selected Hydrogen Bonds Data for **EtBpy-Pb_3I_8**.

D–H···A	D–H (Å)	H···A (Å)	D···A (Å)	∠(DHA) (°)
C2-H2···I7[a]	0.93	2.911	3.700	143.57
C4-H4···I7[b]	0.93	2.908	3.768	154.38
C11-H11A···I1[c]	0.97	3.060	3.920	148.53
C11-H11B···I6[d]	0.97	3.068	3.949	151.75

Symmetry code: a (x-1/2, -y+1/2, z+1/2), b (x-1, y, z), c (x-1/2, -y+1/2, z-1/2), d (x-1/2, -y+1/2, z+1/2).

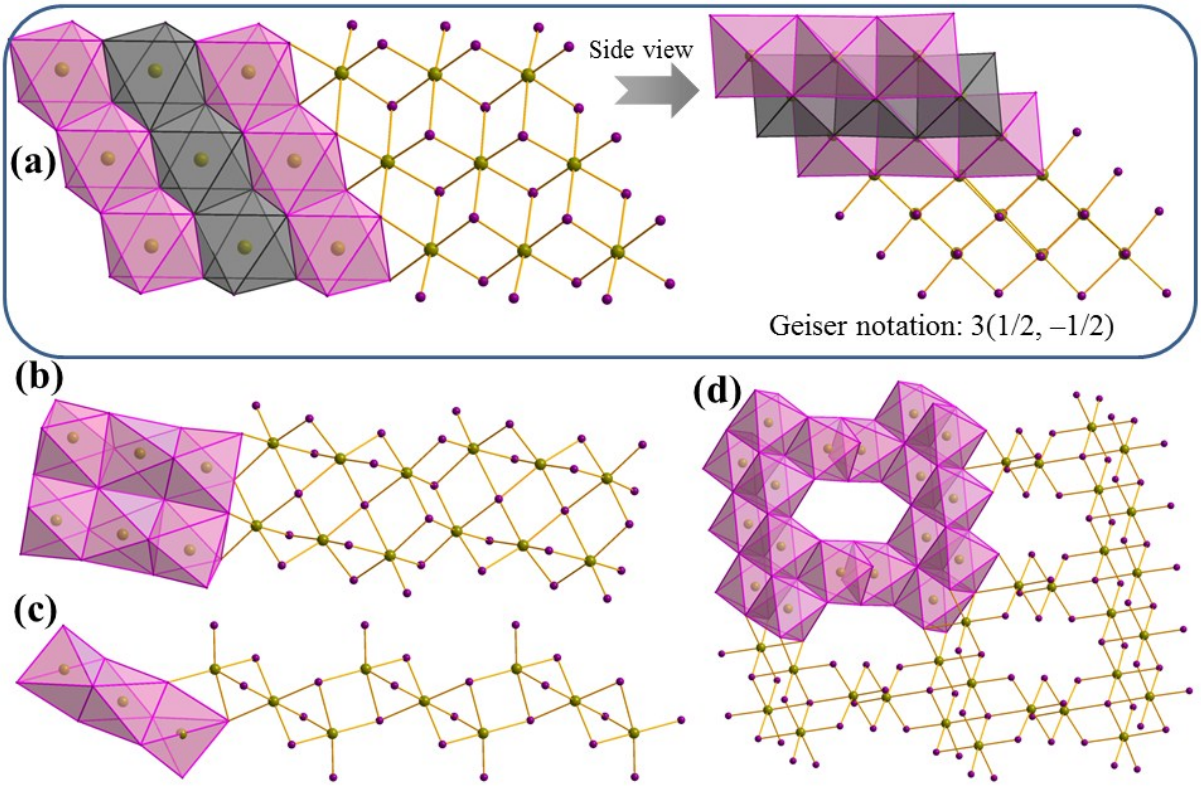

Fig. S3 Four isomers of inorganic $(Pb_3I_8)^{2-}$ polyanions. Type (a) is the most related chain, which is built by the stacks of the trinuclear (Pb_3I_{14}) building units, but with a different Gerser notation of 3(1/2, –1/2).

Although several $(Pb_3I_8)^{2-}$ anionic chains have been reported, they show different condensations of the (PbI_6) octahedra.[6] The $(Pb_3I_8)^{2-}$ anionic chain in **EtBpy-Pb_3I_8** also differ from the most related inorganic chain, which also shows the stacking of trinuclear (Pb_3I_{14}) units, but has a Gerser notation of 3(1/2, –1/2), as shown in Fig. S3.[6c]

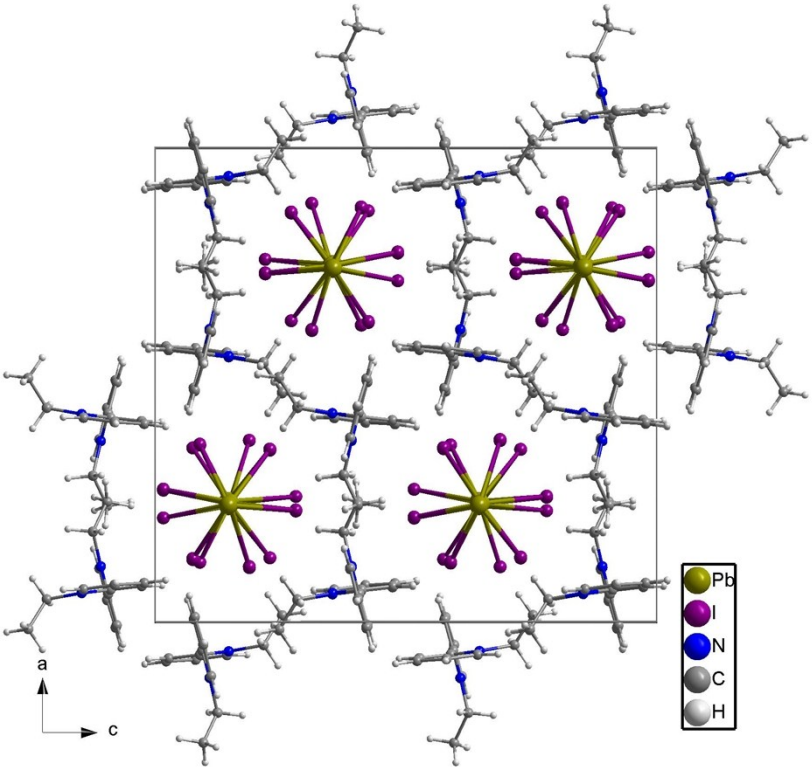

Fig. S4 The 3D packing diagram of **EtBpy-Pb_2I_6**.

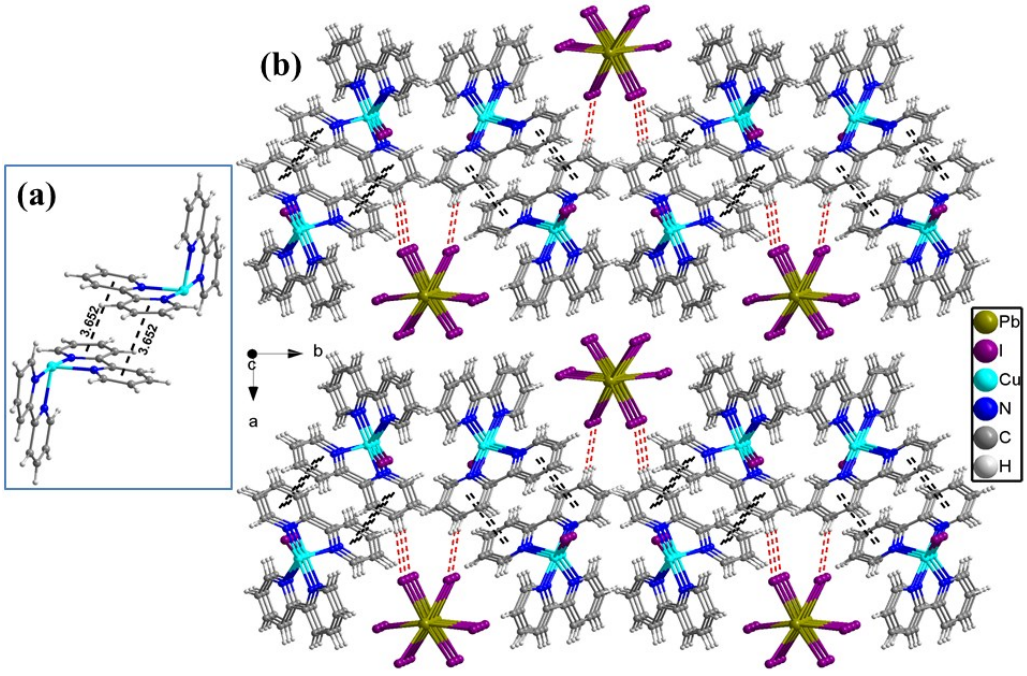

Fig. S5 (a) The $[Cu^{II}(Bpy)_2I]_2^{2+}$ pairs with face to face π···π stacking interactions (black dashed lines). (b) The 3D packing diagram of **CuIBpy-Pb_2I_6**. Hydrogen bonds are shown in red dashed lines.

Table S4 Selected Hydrogen Bonds Data for **CuIBpy-Pb_2I_6**.

D–H···A	D–H (Å)	H···A (Å)	D···A (Å)	∠(DHA) (°)
C20-H20···I4	0.93	3.062	3.512	111.51

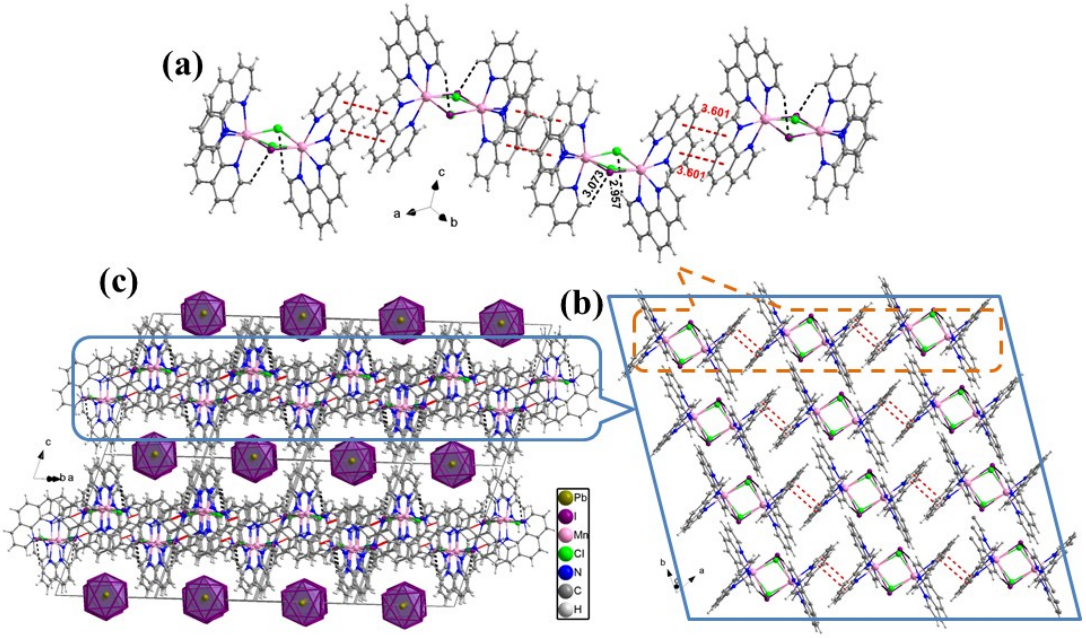

Fig. S6 (a) The 1D supramolecular $[Mn^{II}(phen)_2Cl_{0.65}I_{0.35}]_{2n}^{2n+}$ chains in **bi-MnPhen-Pb_2I_6** formed via face to face π···π stacking interactions (shown as red dashed line). The C–H···I hydrogen bonds within the binuclear cations are shown in black dashed lines. (b) The 2D metal complex cationic layer formed by the side by side aggregation of the 1D supramolecular $[Mn^{II}_2(phen)_4(Cl_{0.65}I_{0.35})_2]_n^{2n+}$ chains in the *ab* plane. (c) The 3D supramolecular framework stabilized by the Coulomb interactions between the organic and inorganic components.

Detail structural description of the $(Pb_2I_6)^{2-}$ chains in EtBpy-Pb_2I_6, CuIBpy-Pb_2I_6 and bi-MnPhen-Pb_2I_6

Each Pb atom in the inorganic chain is coordinated by six μ_2-I atoms to form a distorted Pb-centered octahedron. The axial trans I–Pb–I bond angles are in the range of 167.62(1)–168.97(1)°, 169.53(1)–175.28(1)°, and 172.56(1)–180.0° respectively, indicative of the more serious distortions of the (PbI_6) octahedra in **EtBpy-Pb_2I_6** than those in **CuIBpy-Pb_2I_6** and **bi-MnPhen-Pb_2I_6**. The I atoms all act as μ_2 ligands linking two Pb atoms from two

neighboring (PbI_6) octahedra, where the Pb–μ_2-I bond distances are in the range of 3.123(1)–3.406(1) Å, 3.185(1)–3.303(1) Å, and 3.196(1)–3.378(1) Å, respectively. The 1D $(Pb_2I_6)^{2-}$ chains expand along the *b*, *c* and the [-110] direction with the diameters of 5.165, 5.115, and 5.477 Å, respectively.

Table S5 Selected Hydrogen Bonds Data for **bi-MnPhen-Pb_2I_6**.

D–H···A	D–H (Å)	H···A (Å)	D···A (Å)	∠(DHA) (°)
C22–H22···I8A	0.930	3.073	3.765	132.54
C25–H25···I7A	0.930	2.957	3.655	133.06

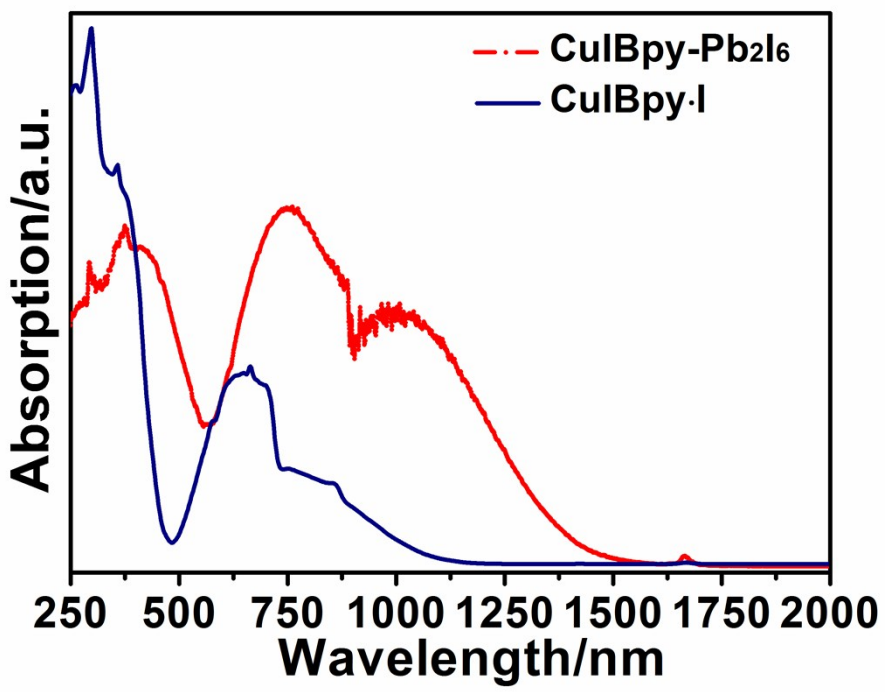

Fig. S7 Comparison of the absorption spectra of **CuIBpy-Pb_2I_6** and CuIBpy·I.

Table S6 Energy band-gaps of the mostly reported widely used perovskite light absorbers.[7]

Perovskite light absorbers	**Band Gaps/eV**
$CH_3NH_3PbCl_3$	3.11
$CH_3NH_3PbBr_3$	2.3

$Cs_3Bi_2I_9$	2.2
$CH_3NH_3Bi_2I_9$	2.1
$CsSb_2I_9$	2.05
$CH_3NH_3GeI_3$	1.9
$FA_{0.83}Cs_{0.17}Pb(I_{0.5}Br_{0.5})_3$	1.8
$CsPbI_3$	1.73
$CsGeI_3$	1.6
$CH_3NH_3PbI_3$	1.55
$CH(NH_2)_2PbI_3$	1.48
$CH_3NH_3SnI_3$	1.3
$FA_{0.75}Cs_{0.25}Sn_{0.5}Pb_{0.5}I_3$	1.2
$CH_3NH_3Sn_{0.5}Pb_{0.5}I_3$	1.17

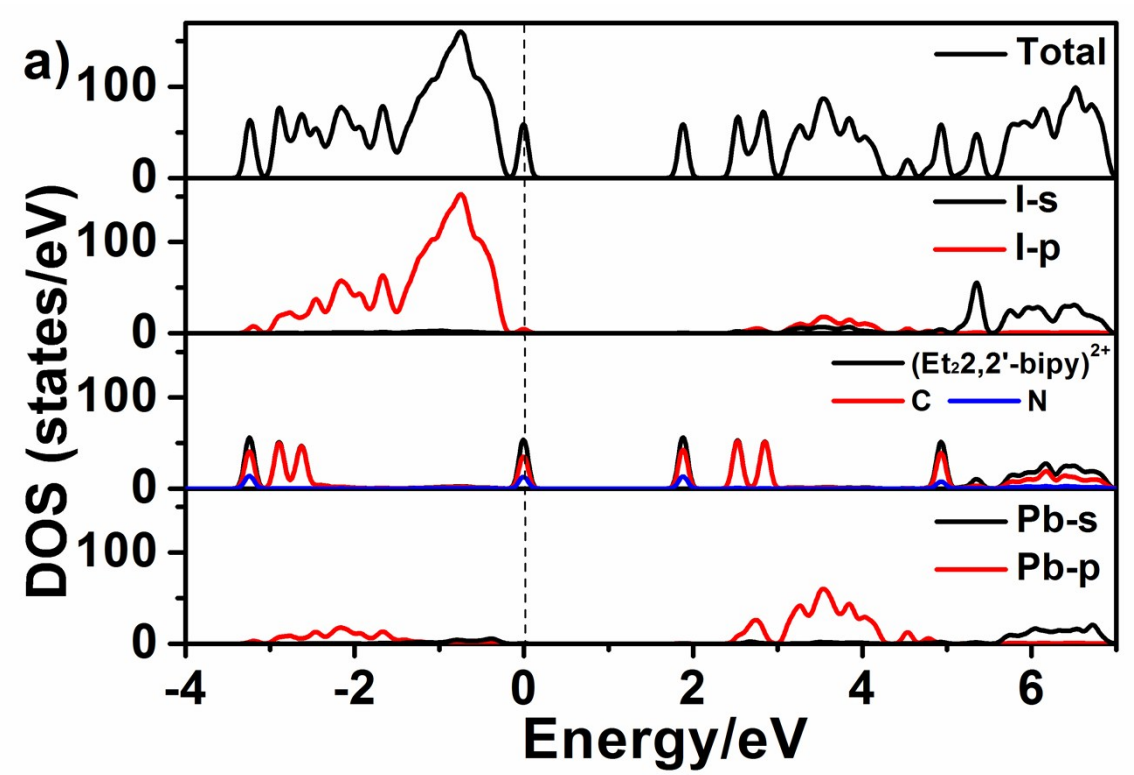

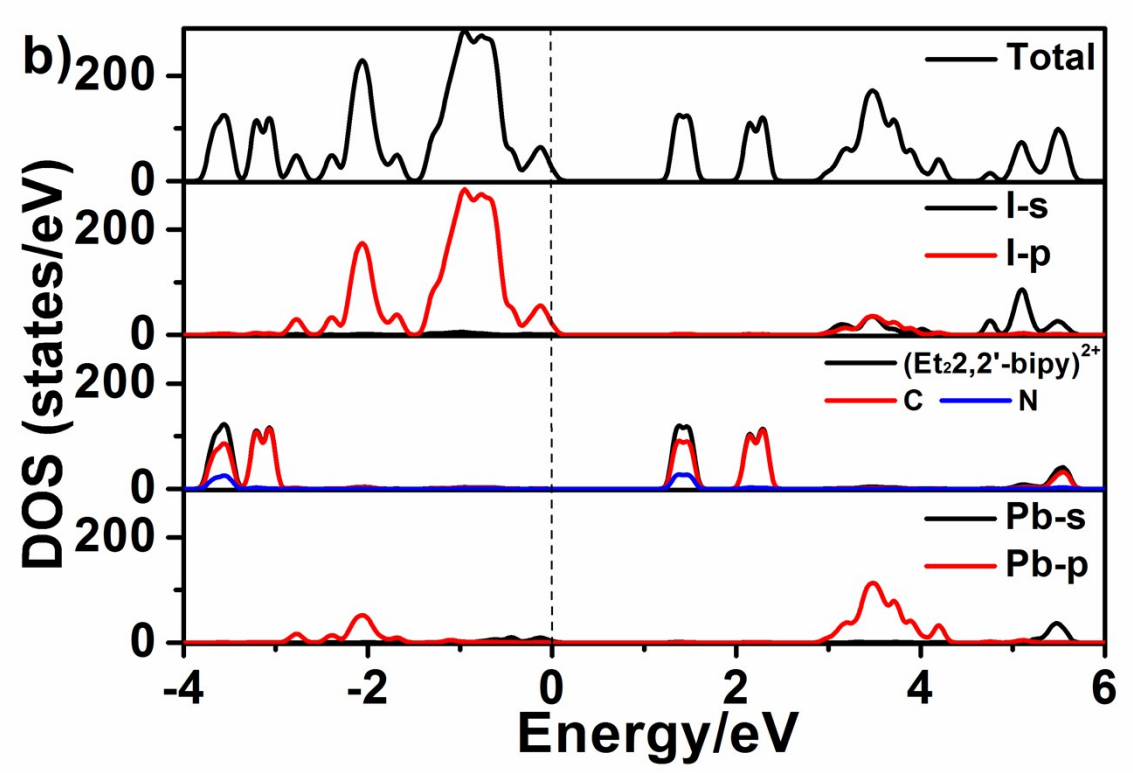
b)
Total
I-s
I-p
(Et2,2'-bipy)2+
C
N
Pb-s
Pb-p
DOS (states/eV)
Energy/eV

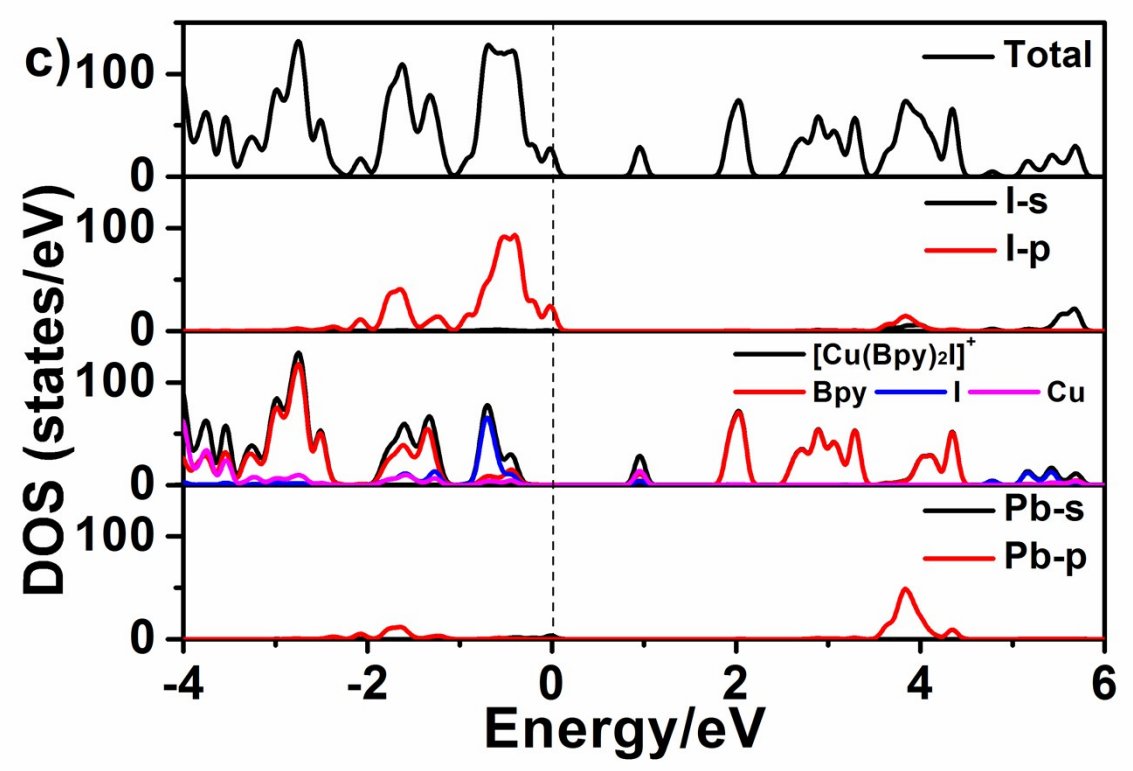
c)
Total
I-s
I-p
[Cu(Bpy)2I]+
Bpy
I
Cu
Pb-s
Pb-p
DOS (states/eV)
Energy/eV

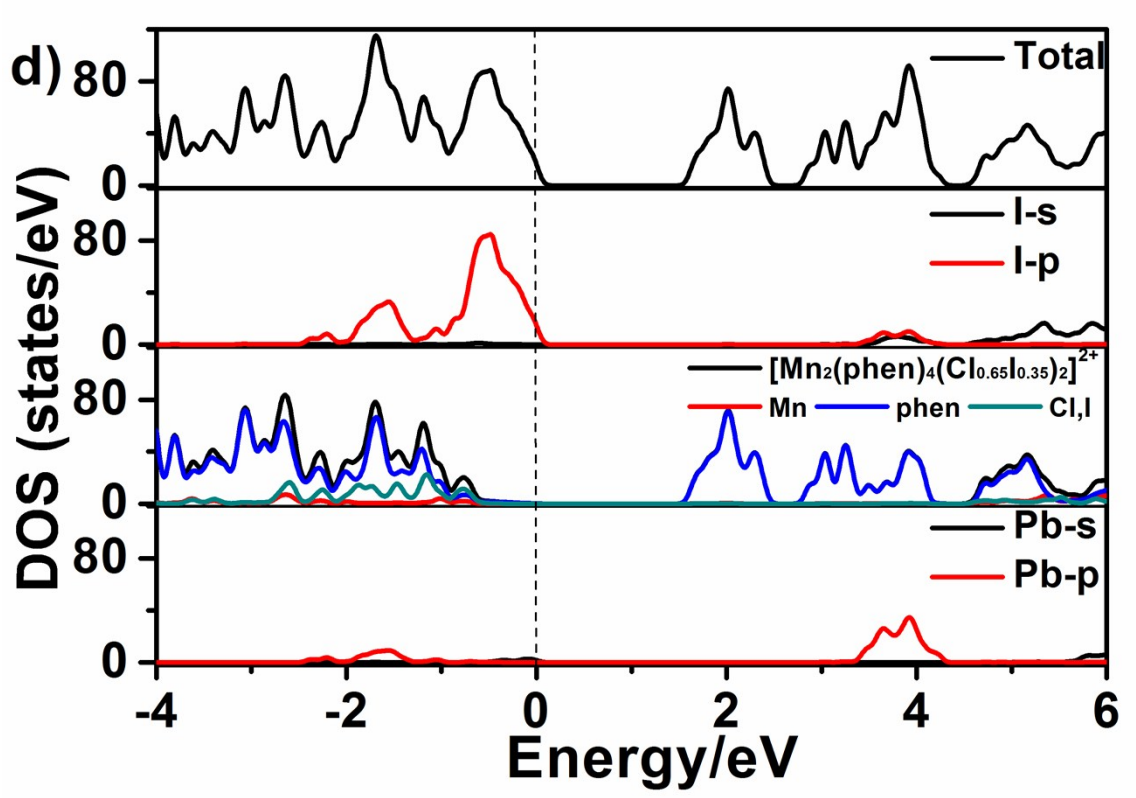

Fig. S8 The total and partial DOS of **EtBpy-Pb_3I_8** (a), **EtBpy-Pb_2I_6** (b), **CuIBpy-Pb_2I_6** (c), **bi-MnPhen-Pb_2I_6** (d). The Fermi level is set to zero by default.

S4 A detail discussion of the electronic structures of bi-MnPhen-Pb_2I_6 and CuIBpy-Pb_2I_6

Hybrid **bi-MnPhen-Pb_2I_6** shows a slight different electronic structure from that of **CuIBpy-Pb_2I_6**, which is reflected in the bottom of the CBs (Fig.s S7c and S7d). The top of VBs closest to Fermi energy (–2 and 0 eV) include the contributions of 5p state of I and a little contribution from bi-Mn complex. The contribution of bi-Mn complex in **bi-MnPhen-Pb_2I_6** is relative smaller than the Cu complex to the top of VBs in **CuIBpy-Pb_2I_6**, which implies the lower-lying of the highest occupied molecular orbitals of bi-Mn complex. The bi-Mn complex constitutes nearly all the bottom of the CBs between 0 and 3 eV, however the Phen ligands make a major contribution, and the contributions from Mn and bridging I (denoted as b-I) and Cl atoms are negligible. Therefore, the optical absorptions are mainly ascribed to the charge transitions from 5p state of I to the p-π* orbitals of Phen ligand.

Table S7 The calculated molecular orbitals of related organic cations.

Organic cation	HOMO energy/ hartrees	LUMO energy/ hartrees	Energy gap between HOMO and LUMO/ hartrees
$(Et_2Bpy)^{2+}$	-0.57282	-0.35849	0.2143
$[Cu(en)_3]^{2+}$	-0.51415	-0.23851	0.2756
$[Cu(Bpy)_2I]^{+}$	-0.31057	-0.18983	0.1207
$[Cu(Bpy)_3]^{2+}$	-0.44589	-0.28002	0.1659
$[Mn(en)_3]^{2+}$	-0.48513	-0.24108	0.2441
[a]$[Mn(Phen)_2Cl_{0.65}I_{0.35}]_2^{2+}$	-0.38349	-0.23271	0.1508
$[Mn(Phen)_2Cl_2]_2^{2+}$	-0.38879	-0.23244	0.1564
$[Mn_2(Phen)_4ClI]_2^{2+}$	-0.37364	-0.23321	0.1404
$[Mn_2(Phen)_4I_2]_2^{2+}$	-0.3638	-0.23294	0.1309

[a]The molecular orbital energies of $[Mn(Phen)_2Cl_{0.65}I_{0.35}]_2^{2+}$ were calculated from the energies of $[Mn(Phen)_2Cl]_2^{2+}$ and $[Mn(Phen)_2I]_2^{2+}$ according to the stoichiometries of Cl and I bridges.

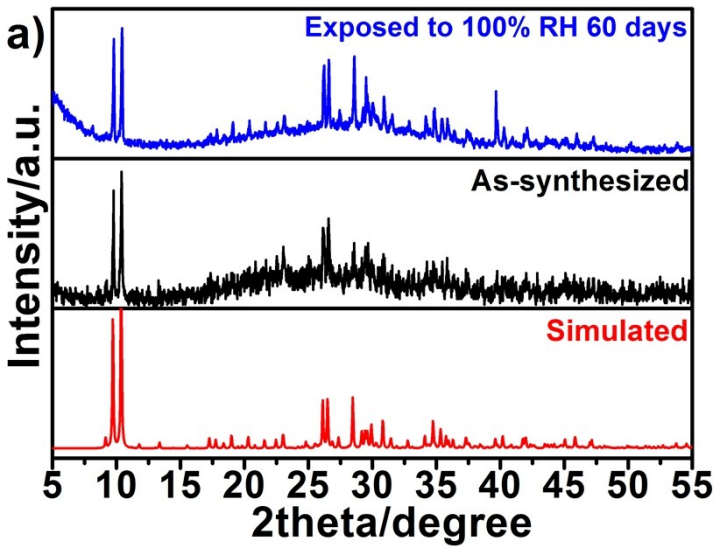

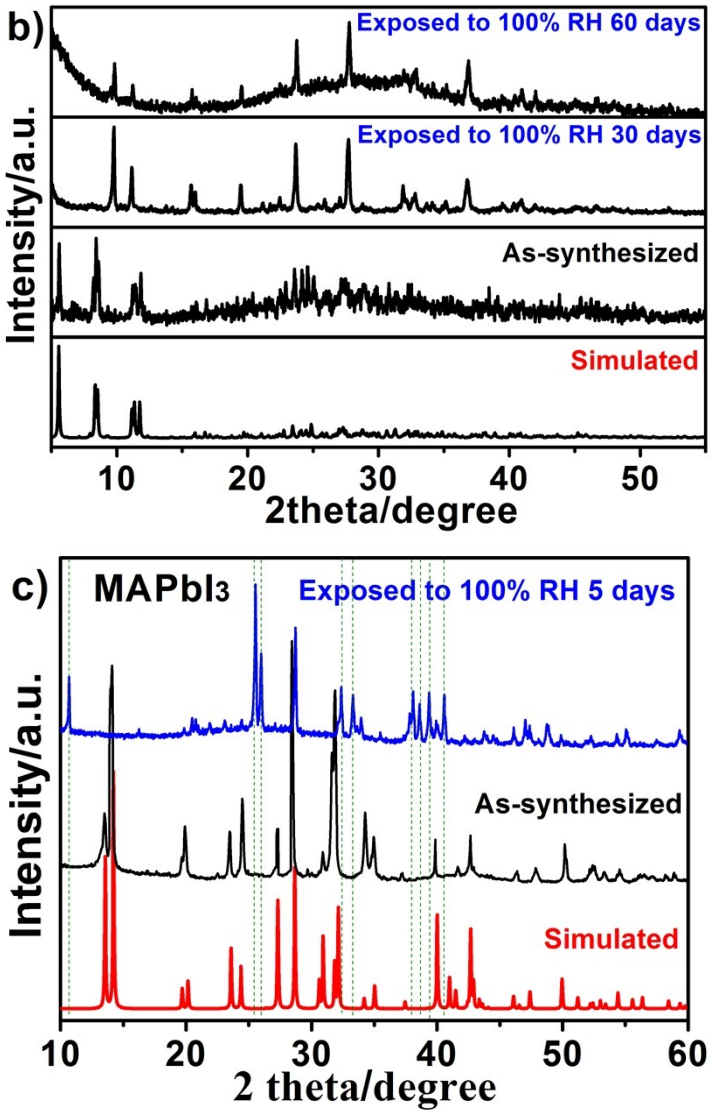

Fig. S9 Experimental and simulated PXRD patterns of (a) **EtBpy-Pb_2I_6**, (b) **bi-MnPhen-Pb_2I_6** and (c) **$MAPbI_3$**.

S5. Additional stability studies

The PXRD pattern in Fig. S8a shows the main PXRD peaks of **EtBpy-Pb_2I_6** after 100% RH treatment agree well with its freshly synthesized sample, indicating its enhanced moisture stability. Comparatively, **bi-MnPhen-Pb_2I_6** has inferior moisture stability; because a new phase occurred in the sample despite the irradiation time was reduced to 30 days (Fig. S8b). As shown in Fig. S8c, the well-known methylamine lead iodine has the worst moisture stability, the unmatched peaks occurred only after in 100% TH for 5 days.

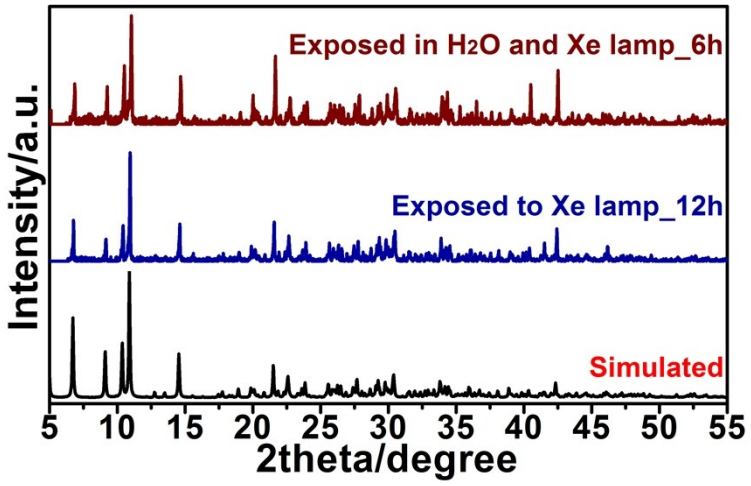

Fig. S10 Additional stability evaluation for **CuIBpy-Pb_2I_6**, which further indicates its enhanced photostability and moisture stability.

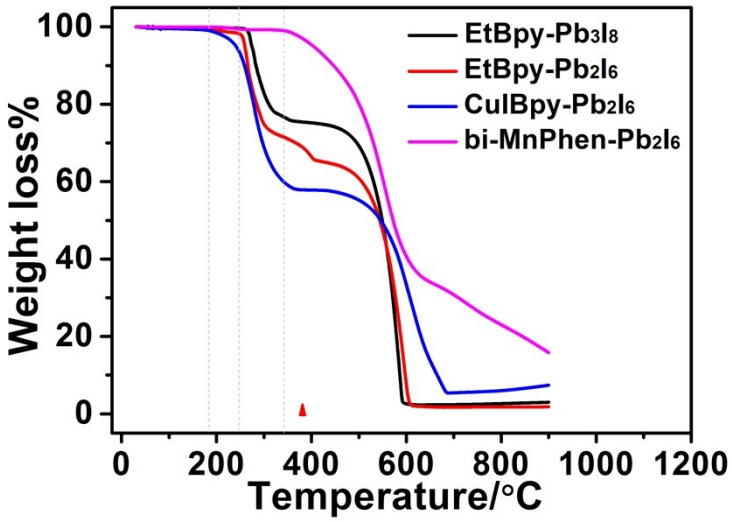

Fig. S11 TGA curves for four involved lead iodine hybrids. The TGA under N_2 atmosphere in the temperature range of 313–1273 K suggest that **EtBpy-Pb_2I_6**, and **bi-MnPhen-Pb_2I_6** are stable up to 521 K and 611 K respectively, confirming their excellent thermal stabilities.

S6. Fabrication details of the photoelectrochemical device

The photoelectrochemical test was performed using an Au interdigital electrode. Before its use, the electrode was carefully cleaned by ethanol and dried at 40 °C for 30 min. A 10 $mg \cdot mL^{-1}$ suspension of sample powder was prepared using ethanol as the solvent. The as-prepared suspension was homogeneous dispersed using ball milling. Then, 3.5 μL-suspension was deposited onto Au interdigital electrode by drop-casting method for 5 times to form a

uniform film. The film-electrode was dried at 40 °C for 4 hours in a vacuum oven. For the following photocurrent measurements, a 500 W Xe lamp was chosen as the light source. The photoresponse results were recorded by a Solartron ModuLab XM.

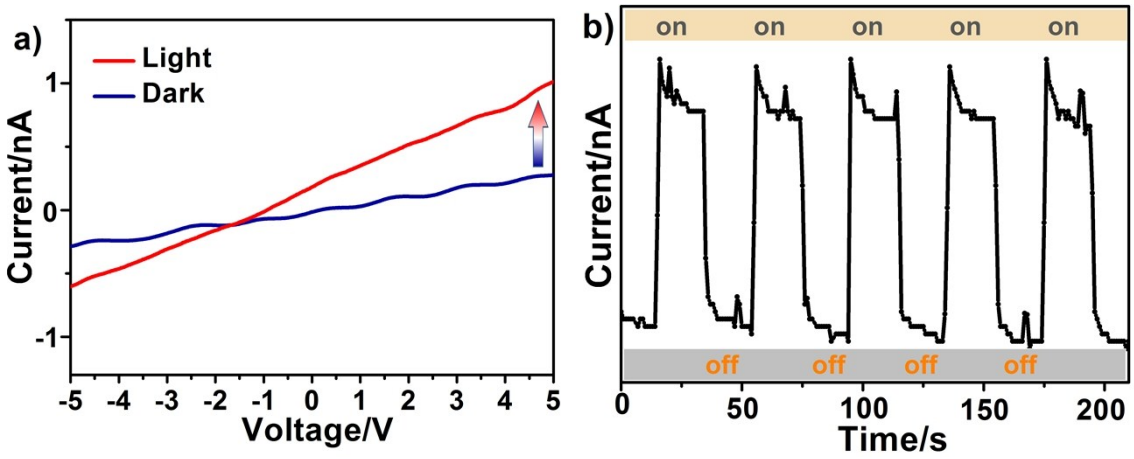

Fig. S12 (a) The current-voltage curves of **bi-MnPhen-Pb_2I_6** in the dark, and under a 500 W Xe lamp. (b) Time-dependent photoresponse showing the excellent repeatability.

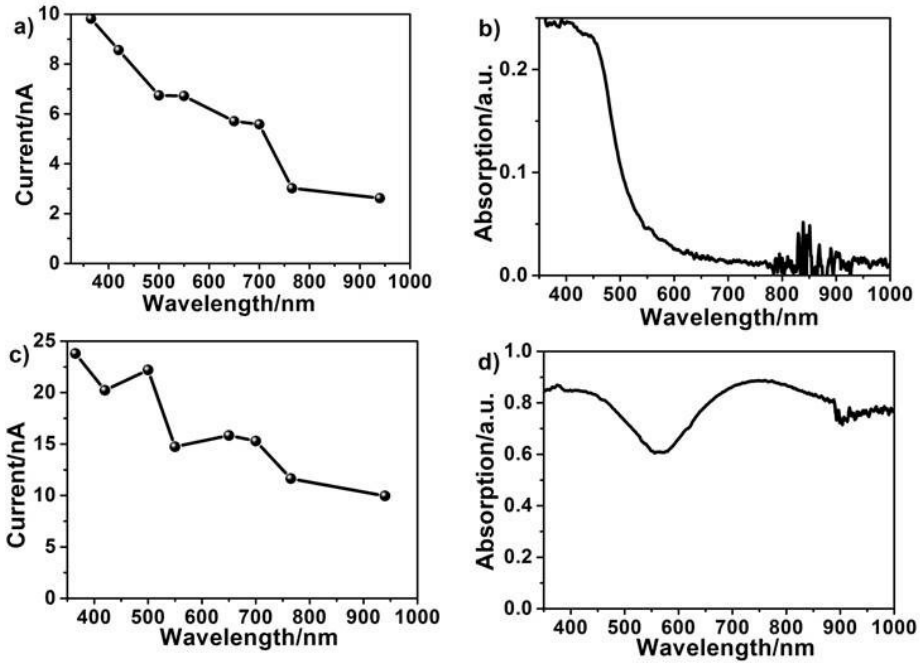

Fig. S13 The photocurrent of the film device at different wavelengths with a bias of 5.0 V and optical absorption spectra for **EtBpy-Pb_3I_8** (a, b) and **CuIBpy-Pb_2I_6** (c, d).

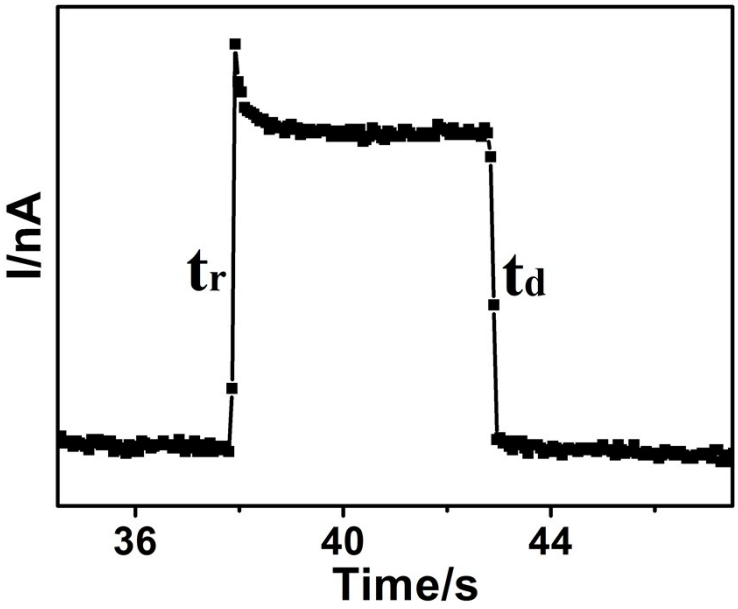

Fig. S14 The response time of the photoconductive device based on **CuIBpy-Pb_2I_6**.

Table S8 Selected Bond Distances (Å) and Angles (°).

EtBpy-Pb_3I_8			
Bond	(Å)	Bond	(Å)
Pb(1)-I(1)	2.9847(3)	I(8)-Pb(1)#2	3.2197(3)
Pb(1)-I(2)	3.2652(3)	N(1)-C(1)	1.333(5)
Pb(1)-I(6)#1	3.0929(3)	N(1)-C(5)	1.316(5)
Pb(1)-I(8)#2	3.2197(3)	N(1)-C(11)	1.524(5)
Pb(2)-I(2)	3.1068(3)	N(2)-C(6)	1.363(4)
Pb(2)-I(3)	3.2259(2)	N(2)-C(10)	1.321(5)
Pb(2)-I(3)#3	3.3610(3)	N(2)-C(13)	1.538(6)
Pb(2)-I(4)	3.1295(3)	C(1)-C(2)	1.369(6)
Pb(2)-I(5)#1	3.3411(2)	C(2)-C(3)	1.439(6)
Pb(2)-I(5)	3.2220(3)	C(3)-C(4)	1.334(6)
Pb(3)-I(4)#4	3.2633(3)	C(4)-C(5)	1.378(5)
Pb(3)-I(5)	3.3921(3)	C(5)-C(6)	1.510(5)
Pb(3)-I(6)	3.2179(3)	C(6)-C(7)	1.333(5)
Pb(3)-I(7)	3.0110(3)	C(7)-C(8)	1.385(5)

Pb(3)-I(8)	3.0957(3)	C(8)-C(9)	1.348(5)
I(3)-Pb(2)#3	3.3611(3)	C(9)-C(10)	1.341(5)
I(4)-Pb(3)#5	3.2633(3)	C(13)-C(14)	1.407(7)
I(5)-Pb(2)#1	3.3412(2)	C(11)-C(12)	1.437(6)
I(6)-Pb(1)#1	3.0930(3)		
Angle	(°)	Angle	(°)
I(1)-Pb(1)-I(2)	95.685(8)	Pb(2)-I(2)-Pb(1)	96.121(7)
I(1)-Pb(1)-I(6)#1	89.653(8)	Pb(2)-I(3)-Pb(2)#3	93.180(6)
I(1)-Pb(1)-I(8)#2	94.855(9)	Pb(2)-I(4)-Pb(3)#5	94.704(7)
I(6)#1-Pb(1)-I(2)	90.805(7)	Pb(2)-I(5)-Pb(2)#1	90.682(6)
I(6)#1-Pb(1)-I(8)#2	96.791(7)	Pb(2)#1-I(5)-Pb(3)	93.059(6)
I(8)#2-Pb(1)-I(2)	167.035(8)	Pb(2)-I(5)-Pb(3)	174.044(8)
I(2)-Pb(2)-I(3)#3	175.703(7)	Pb(1)#1-I(6)-Pb(3)	98.253(8)
I(2)-Pb(2)-I(3)	95.102(7)	Pb(3)-I(8)-Pb(1)#2	95.856(8)
I(2)-Pb(2)-I(4)	93.540(7)	C(1)-N(1)-C(11)	115.8(3)
I(2)-Pb(2)-I(5)#1	90.845(6)	C(5)-N(1)-C(1)	121.7(3)
I(2)-Pb(2)-I(5)	91.970(7)	C(5)-N(1)-C(11)	122.5(3)
I(3)-Pb(2)-I(3)#3	86.820(6)	C(6)-N(2)-C(13)	123.4(3)
I(3)-Pb(2)-I(5)#1	88.313(6)	C(10)-N(2)-C(6)	120.8(3)
I(4)-Pb(2)-I(3)	88.938(7)	C(10)-N(2)-C(13)	115.7(3)
I(4)-Pb(2)-I(3)#3	90.335(7)	N(1)-C(1)-C(2)	120.5(4)
I(4)-Pb(2)-I(5)#1	175.016(7)	C(1)-C(2)-C(3)	119.8(4)
I(4)-Pb(2)-I(5)	92.895(7)	C(4)-C(3)-C(2)	114.1(4)
I(5)#1-Pb(2)-I(3)#3	85.363(6)	C(3)-C(4)-C(5)	125.0(4)
I(5)-Pb(2)-I(3)	172.573(7)	N(1)-C(5)-C(4)	118.0(4)
I(5)-Pb(2)-I(3)#3	85.973(6)	N(1)-C(5)-C(6)	117.8(3)
I(5)-Pb(2)-I(5)#1	89.317(6)	C(4)-C(5)-C(6)	123.8(3)

I(4)#4-Pb(3)-I(5)	85.265(7)	N(2)-C(6)-C(5)	118.9(3)
I(6)-Pb(3)-I(4)#4	167.033(7)	C(7)-C(6)-N(2)	118.6(3)
I(6)-Pb(3)-I(5)	86.879(7)	C(7)-C(6)-C(5)	121.4(3)
I(7)-Pb(3)-I(4)#4	93.435(8)	C(6)-C(7)-C(8)	120.5(3)
I(7)-Pb(3)-I(5)	92.801(7)	C(9)-C(8)-C(7)	119.2(4)
I(7)-Pb(3)-I(6)	97.241(8)	C(10)-C(9)-C(8)	119.3(4)
I(7)-Pb(3)-I(8)	92.793(8)	N(2)-C(10)-C(9)	121.3(3)
I(8)-Pb(3)-I(4)#4	97.590(9)	C(14)-C(13)-N(2)	110.1(4)
I(8)-Pb(3)-I(5)	173.555(7)	C(12)-C(11)-N(1)	110.4(3)
I(8)-Pb(3)-I(6)	89.244(8)		

Symmetry transformations used to generate equivalent atoms: #1 -x+2, -y, -z+1; #2 -x+1, -y, -z+1; #3 -x+3, -y, -z+1; #4 x-1, y, z; #5 x+1, y, z.

EtBpy-Pb_2I_6			
Bond	(Å)	Bond	(Å)
Pb(1)-I(1)	3.2361(4)	N(1)-C(5)	1.328(7)
Pb(1)-I(2)	3.1767(4)	N(1)-C(11)	1.499(7)
Pb(1)-I(3)	3.4061(5)	N(2)-C(6)	1.363(6)
Pb(1)-I(4)	3.2389(5)	N(2)-C(10)	1.347(6)
Pb(1)-I(5)	3.3433(5)	N(2)-C(13)	1.506(7)
Pb(1)-I(6)	3.1633(5)	C(1)-C(2)	1.385(8)
Pb(2)-I(1)#1	3.2466(4)	C(2)-C(3)	1.338(8)
Pb(2)-I(2)#1	3.2476(4)	C(3)-C(4)	1.396(7)
Pb(2)-I(3)#1	3.1226(5)	C(4)-C(5)	1.378(8)
Pb(2)-I(4)	3.2195(5)	C(5)-C(6)	1.489(6)
Pb(2)-I(5)	3.1689(5)	C(6)-C(7)	1.362(7)
Pb(2)-I(6)	3.3159(5)	C(7)-C(8)	1.399(7)
I(1)-Pb(2)#2	3.2466(4)	C(8)-C(9)	1.349(7)

I(2)-Pb(2)#2	3.2476(4)	C(9)-C(10)	1.358(8)
I(3)-Pb(2)#2	3.1227(5)	C(11)-C(12)	1.433(9)
N(1)-C(1)	1.346(6)	C(13)-C(14)	1.451(9)
Angle	(°)	Angle	(°)
I(1)-Pb(1)-I(3)	84.863(11)	I(5)-Pb(2)-I(6)	86.685(12)
I(1)-Pb(1)-I(4)	168.970(13)	Pb(1)-I(1)-Pb(2)#2	75.945(11)
I(1)-Pb(1)-I(5)	84.629(12)	Pb(1)-I(2)-Pb(2)#2	76.752(11)
I(2)-Pb(1)-I(1)	86.570(12)	Pb(2)#2-I(3)-Pb(1)	75.176(11)
I(2)-Pb(1)-I(3)	83.503(11)	Pb(2)-I(4)-Pb(1)	74.817(11)
I(2)-Pb(1)-I(4)	101.826(13)	Pb(2)-I(5)-Pb(1)	74.042(11)
I(2)-Pb(1)-I(5)	167.617(13)	Pb(1)-I(6)-Pb(2)	74.495(11)
I(4)-Pb(1)-I(3)	88.958(12)	C(1)-N(1)-C(11)	117.0(4)
I(4)-Pb(1)-I(5)	88.070(12)	C(5)-N(1)-C(1)	122.3(5)
I(5)-Pb(1)-I(3)	104.320(12)	C(5)-N(1)-C(11)	120.7(4)
I(6)-Pb(1)-I(1)	101.406(12)	C(6)-N(2)-C(13)	119.9(4)
I(6)-Pb(1)-I(2)	86.916(12)	C(10)-N(2)-C(6)	121.2(4)
I(6)-Pb(1)-I(3)	168.231(13)	C(10)-N(2)-C(13)	118.8(4)
I(6)-Pb(1)-I(4)	86.325(12)	N(1)-C(1)-C(2)	119.2(5)
I(6)-Pb(1)-I(5)	86.307(12)	C(3)-C(2)-C(1)	119.7(4)
I(1)#1-Pb(2)-I(2)#1	85.227(11)	C(2)-C(3)-C(4)	120.4(5)
I(1)#1-Pb(2)-I(6)	89.861(11)	C(5)-C(4)-C(3)	118.5(5)
I(2)#1-Pb(2)-I(6)	97.942(12)	N(1)-C(5)-C(4)	119.8(4)
I(3)#1-Pb(2)-I(1)#1	89.460(12)	N(1)-C(5)-C(6)	119.7(5)
I(3)#1-Pb(2)-I(2)#1	87.023(12)	C(4)-C(5)-C(6)	120.3(5)
I(3)#1-Pb(2)-I(4)	90.912(12)	N(2)-C(6)-C(5)	120.8(4)
I(3)#1-Pb(2)-I(5)	94.667(13)	C(7)-C(6)-N(2)	117.7(4)
I(3)#1-Pb(2)-I(6)	174.915(13)	C(7)-C(6)-C(5)	121.1(5)

I(4)-Pb(2)-I(1)#1	96.013(13)	C(6)-C(7)-C(8)	121.5(5)
I(4)-Pb(2)-I(2)#1	177.585(13)	C(9)-C(8)-C(7)	118.1(5)
I(4)-Pb(2)-I(6)	84.148(12)	C(8)-C(9)-C(10)	120.5(5)
I(5)-Pb(2)-I(1)#1	171.379(13)	N(2)-C(10)-C(9)	120.6(5)
I(5)-Pb(2)-I(2)#1	87.429(12)	C(12)-C(11)-N(1)	116.8(5)
I(5)-Pb(2)-I(4)	91.493(13)	C(14)-C(13)-N(2)	114.0(5)

Symmetry transformations used to generate equivalent atoms: #1 -x+3/2, y+1/2, z; #2 -x+3/2, y-1/2, z.

CuIBpy-Pb_2I_6			
Bond	(Å)	Bond	(Å)
Pb(1)-I(1)	3.1848(3)	N(4)-C(16)	1.329(6)
Pb(1)-I(1)#1	3.1852(3)	N(4)-C(20)	1.332(7)
Pb(1)-I(2)#1	3.2820(3)	C(1)-C(2)	1.398(6)
Pb(1)-I(2)	3.2722(3)	C(2)-C(3)	1.371(7)
Pb(1)-I(3)#2	3.1922(3)	C(3)-C(4)	1.349(7)
Pb(1)-I(3)	3.3033(4)	C(4)-C(5)	1.408(5)
I(1)-Pb(1)#2	3.1852(3)	C(5)-C(6)	1.481(6)
I(2)-Pb(1)#2	3.2819(3)	C(6)-C(7)	1.387(6)
I(3)-Pb(1)#1	3.1922(3)	C(7)-C(8)	1.363(7)
I(4)-Cu(1)	2.6218(6)	C(8)-C(9)	1.344(6)
Cu(1)-N(1)	1.994(3)	C(9)-C(10)	1.391(7)
Cu(1)-N(2)	2.124(3)	C(11)-C(12)	1.374(7)
Cu(1)-N(3)	2.091(3)	C(12)-C(13)	1.331(8)
Cu(1)-N(4)	1.983(3)	C(13)-C(14)	1.341(9)
N(1)-C(1)	1.322(5)	C(14)-C(15)	1.479(7)
N(1)-C(5)	1.352(5)	C(15)-C(16)	1.421(7)
N(2)-C(6)	1.339(4)	C(16)-C(17)	1.406(7)

N(2)-C(10)	1.317(6)	C(17)-C(18)	1.311(9)
N(3)-C(11)	1.330(6)	C(18)-C(19)	1.360(9)
N(3)-C(15)	1.337(5)	C(19)-C(20)	1.496(8)
Angle	(°)	Angle	(°)
I(1)-Pb(1)-I(1)#1	96.213(10)	C(11)-N(3)-Cu(1)	126.4(3)
I(1)-Pb(1)-I(2)#1	175.280(9)	C(11)-N(3)-C(15)	121.5(4)
I(1)#1-Pb(1)-I(2)#1	87.924(8)	C(15)-N(3)-Cu(1)	111.8(3)
I(1)#1-Pb(1)-I(2)	174.734(9)	C(16)-N(4)-Cu(1)	114.5(3)
I(1)-Pb(1)-I(2)	88.099(8)	C(16)-N(4)-C(20)	123.3(4)
I(1)#1-Pb(1)-I(3)#2	87.935(9)	C(20)-N(4)-Cu(1)	122.0(3)
I(1)-Pb(1)-I(3)#2	84.849(9)	N(1)-C(1)-C(2)	122.3(4)
I(1)-Pb(1)-I(3)	90.847(9)	C(3)-C(2)-C(1)	118.4(5)
I(1)#1-Pb(1)-I(3)	83.041(9)	C(4)-C(3)-C(2)	119.2(4)
I(2)-Pb(1)-I(2)#1	87.894(9)	C(3)-C(4)-C(5)	121.2(4)
I(2)#1-Pb(1)-I(3)	87.391(8)	N(1)-C(5)-C(4)	118.7(4)
I(2)-Pb(1)-I(3)	99.962(9)	N(1)-C(5)-C(6)	116.8(3)
I(3)#2-Pb(1)-I(2)#1	97.604(9)	C(4)-C(5)-C(6)	124.5(4)
I(3)#2-Pb(1)-I(2)	89.448(9)	N(2)-C(6)-C(5)	114.8(3)
I(3)#2-Pb(1)-I(3)	169.533(10)	N(2)-C(6)-C(7)	120.9(4)
Pb(1)-I(1)-Pb(1)#2	76.401(7)	C(7)-C(6)-C(5)	124.2(3)
Pb(1)-I(2)-Pb(1)#2	73.889(7)	C(8)-C(7)-C(6)	118.6(4)
Pb(1)#1-I(3)-Pb(1)	74.647(8)	C(9)-C(8)-C(7)	121.3(5)
N(1)-Cu(1)-I(4)	92.13(9)	C(8)-C(9)-C(10)	116.9(5)
N(1)-Cu(1)-N(2)	80.25(12)	N(2)-C(10)-C(9)	123.5(4)
N(1)-Cu(1)-N(3)	95.18(12)	N(3)-C(11)-C(12)	123.7(5)
N(2)-Cu(1)-I(4)	125.77(8)	C(13)-C(12)-C(11)	114.1(6)
N(3)-Cu(1)-I(4)	135.11(10)	C(12)-C(13)-C(14)	128.3(6)

N(3)-Cu(1)-N(2)	99.11(13)	C(13)-C(14)-C(15)	114.3(5)
N(4)-Cu(1)-I(4)	94.68(11)	N(3)-C(15)-C(14)	118.0(4)
N(4)-Cu(1)-N(1)	173.19(14)	N(3)-C(15)-C(16)	115.5(4)
N(4)-Cu(1)-N(2)	95.76(13)	C(16)-C(15)-C(14)	126.5(4)
N(4)-Cu(1)-N(3)	79.94(14)	N(4)-C(16)-C(15)	117.8(4)
C(1)-N(1)-Cu(1)	124.5(3)	N(4)-C(16)-C(17)	122.6(5)
C(1)-N(1)-C(5)	120.2(3)	C(17)-C(16)-C(15)	119.5(4)
C(5)-N(1)-Cu(1)	115.3(3)	C(18)-C(17)-C(16)	111.2(5)
C(6)-N(2)-Cu(1)	112.4(3)	C(17)-C(18)-C(19)	134.0(6)
C(10)-N(2)-Cu(1)	127.9(3)	C(18)-C(19)-C(20)	109.7(5)
C(10)-N(2)-C(6)	118.6(4)	N(4)-C(20)-C(19)	118.7(5)

Symmetry transformations used to generate equivalent atoms: #1 x, -y+3/2, z+1/2; #2 x, -y+3/2, z-1/2.

bi-MnPhen-Pb_2I_6			
Bond	(Å)	Bond	(Å)
Pb(1)-I(1)#1	3.2873(3)	N(8)-C(47)	1.363(5)
Pb(1)-I(1)	3.2873(3)	C(1)-C(2)	1.398(7)
Pb(1)-I(2)#1	3.1982(3)	C(2)-C(3)	1.338(7)
Pb(1)-I(2)	3.1982(3)	C(3)-C(4)	1.389(6)
Pb(1)-I(3)	3.2253(4)	C(4)-C(5)	1.425(6)
Pb(1)-I(3)#1	3.2253(3)	C(4)-C(12)	1.409(6)
Pb(2)-I(1)	3.2616(4)	C(5)-C(6)	1.352(6)
Pb(2)-I(2)	3.2277(4)	C(6)-C(7)	1.439(7)
Pb(2)-I(3)	3.2371(4)	C(7)-C(8)	1.388(6)
Pb(2)-I(4)	3.2377(3)	C(7)-C(11)	1.429(5)
Pb(2)-I(5)	3.1963(4)	C(8)-C(9)	1.354(7)
Pb(2)-I(6)	3.3770(4)	C(9)-C(10)	1.383(6)

Pb(3)-I(4)#2	3.3152(3)	C(11)-C(12)	1.441(5)
Pb(3)-I(4)	3.3152(3)	C(13)-C(14)	1.391(6)
Pb(3)-I(5)	3.2142(3)	C(14)-C(15)	1.377(6)
Pb(3)-I(5)#2	3.2143(3)	C(15)-C(16)	1.407(5)
Pb(3)-I(6)#2	3.2843(4)	C(16)-C(17)	1.442(6)
Pb(3)-I(6)	3.2843(4)	C(16)-C(24)	1.391(5)
I(7)-Mn(1)	2.8799(10)	C(17)-C(18)	1.332(6)
I(7)-Mn(2)	2.8701(11)	C(18)-C(19)	1.431(6)
I(8)-Mn(1)	2.9141(9)	C(19)-C(20)	1.417(5)
I(8)-Mn(2)	2.9250(9)	C(19)-C(23)	1.395(5)
Mn(1)-Cl(1)	2.5883(17)	C(20)-C(21)	1.354(6)
Mn(1)-Cl(2)	2.5734(15)	C(21)-C(22)	1.381(6)
Mn(1)-N(5)	2.213(3)	C(23)-C(24)	1.445(5)
Mn(1)-N(6)	2.274(3)	C(25)-C(26)	1.387(6)
Mn(1)-N(7)	2.297(3)	C(26)-C(27)	1.352(6)
Mn(1)-N(8)	2.252(3)	C(27)-C(28)	1.417(7)
Mn(2)-Cl(1)	2.5210(18)	C(28)-C(29)	1.445(6)
Mn(2)-Cl(2)	2.6204(15)	C(28)-C(36)	1.395(5)
Mn(2)-N(1)	2.301(3)	C(29)-C(30)	1.331(7)
Mn(2)-N(2)	2.251(3)	C(30)-C(31)	1.435(6)
Mn(2)-N(3)	2.275(3)	C(31)-C(32)	1.400(7)
Mn(2)-N(4)	2.240(3)	C(31)-C(35)	1.409(5)
N(1)-C(1)	1.329(5)	C(32)-C(33)	1.370(6)
N(1)-C(12)	1.363(5)	C(33)-C(34)	1.403(5)
N(2)-C(10)	1.337(5)	C(35)-C(36)	1.437(6)
N(2)-C(11)	1.346(5)	C(37)-C(38)	1.383(6)
N(3)-C(13)	1.328(4)	C(38)-C(39)	1.355(6)
N(3)-C(24)	1.362(5)	C(39)-C(40)	1.406(7)

N(4)-C(22)	1.342(5)	C(40)-C(41)	1.432(7)
N(4)-C(23)	1.364(5)	C(40)-C(48)	1.400(6)
N(5)-C(25)	1.328(6)	C(41)-C(42)	1.332(8)
N(5)-C(36)	1.376(4)	C(42)-C(43)	1.428(6)
N(6)-C(34)	1.342(6)	C(43)-C(44)	1.397(7)
N(6)-C(35)	1.344(5)	C(43)-C(47)	1.398(5)
N(7)-C(37)	1.319(6)	C(44)-C(45)	1.345(7)
N(7)-C(48)	1.359(5)	C(45)-C(46)	1.393(6)
N(8)-C(46)	1.318(6)	C(47)-C(48)	1.456(6)
Angle	(°)	Angle	(°)
I(1)-Pb(1)-I(1)#1	180.0	C(1)-N(1)-C(12)	117.7(4)
I(2)-Pb(1)-I(1)#1	94.046(9)	C(12)-N(1)-Mn(2)	113.9(2)
I(2)#1-Pb(1)-I(1)	94.047(9)	C(10)-N(2)-Mn(2)	126.8(3)
I(2)#1-Pb(1)-I(1)#1	85.954(9)	C(10)-N(2)-C(11)	117.4(3)
I(2)-Pb(1)-I(1)	85.953(9)	C(11)-N(2)-Mn(2)	115.6(2)
I(2)#1-Pb(1)-I(2)	180.0	C(13)-N(3)-Mn(2)	127.5(3)
I(2)-Pb(1)-I(3)#1	91.609(9)	C(13)-N(3)-C(24)	117.8(3)
I(2)#1-Pb(1)-I(3)#1	88.392(8)	C(24)-N(3)-Mn(2)	114.7(2)
I(2)#1-Pb(1)-I(3)	91.608(8)	C(22)-N(4)-Mn(2)	127.4(3)
I(2)-Pb(1)-I(3)	88.392(9)	C(22)-N(4)-C(23)	116.9(3)
I(3)-Pb(1)-I(1)#1	95.249(9)	C(23)-N(4)-Mn(2)	115.4(2)
I(3)-Pb(1)-I(1)	84.751(9)	C(25)-N(5)-Mn(1)	126.9(2)
I(3)#1-Pb(1)-I(1)#1	84.750(9)	C(25)-N(5)-C(36)	118.0(3)
I(3)#1-Pb(1)-I(1)	95.249(9)	C(36)-N(5)-Mn(1)	115.0(3)
I(3)-Pb(1)-I(3)#1	180.0	C(34)-N(6)-Mn(1)	127.9(2)
I(1)-Pb(2)-I(6)	98.499(11)	C(34)-N(6)-C(35)	118.1(3)
I(2)-Pb(2)-I(1)	85.901(9)	C(35)-N(6)-Mn(1)	113.9(3)

I(2)-Pb(2)-I(3)	87.681(9)	C(37)-N(7)-Mn(1)	128.7(3)
I(2)-Pb(2)-I(4)	89.684(9)	C(37)-N(7)-C(48)	117.1(4)
I(2)-Pb(2)-I(6)	99.088(10)	C(48)-N(7)-Mn(1)	113.8(3)
I(3)-Pb(2)-I(1)	84.978(10)	C(46)-N(8)-Mn(1)	126.9(3)
I(3)-Pb(2)-I(4)	99.114(10)	C(46)-N(8)-C(47)	117.0(3)
I(3)-Pb(2)-I(6)	172.564(10)	C(47)-N(8)-Mn(1)	116.0(3)
I(4)-Pb(2)-I(1)	173.865(10)	N(1)-C(1)-C(2)	122.4(4)
I(4)-Pb(2)-I(6)	77.978(9)	C(3)-C(2)-C(1)	119.6(4)
I(5)-Pb(2)-I(1)	93.934(10)	C(2)-C(3)-C(4)	120.8(4)
I(5)-Pb(2)-I(2)	174.841(10)	C(3)-C(4)-C(5)	124.0(4)
I(5)-Pb(2)-I(3)	87.168(10)	C(3)-C(4)-C(12)	116.8(4)
I(5)-Pb(2)-I(4)	90.846(10)	C(12)-C(4)-C(5)	119.3(4)
I(5)-Pb(2)-I(6)	86.040(10)	C(6)-C(5)-C(4)	121.2(5)
I(4)-Pb(3)-I(4)#2	180.0	C(5)-C(6)-C(7)	121.7(4)
I(5)-Pb(3)-I(4)	89.146(8)	C(8)-C(7)-C(6)	124.9(4)
I(5)#2-Pb(3)-I(4)	90.854(9)	C(8)-C(7)-C(11)	116.9(4)
I(5)-Pb(3)-I(4)#2	90.853(9)	C(11)-C(7)-C(6)	118.3(4)
I(5)#2-Pb(3)-I(4)#2	89.146(9)	C(9)-C(8)-C(7)	121.0(4)
I(5)-Pb(3)-I(5)#2	180.0	C(8)-C(9)-C(10)	118.3(4)
I(5)-Pb(3)-I(6)	87.317(10)	N(2)-C(10)-C(9)	124.1(4)
I(5)-Pb(3)-I(6)#2	92.684(9)	N(2)-C(11)-C(7)	122.2(3)
I(5)#2-Pb(3)-I(6)#2	87.315(9)	N(2)-C(11)-C(12)	118.6(3)
I(5)#2-Pb(3)-I(6)	92.684(9)	C(7)-C(11)-C(12)	119.2(4)
I(6)#2-Pb(3)-I(4)#2	78.221(8)	N(1)-C(12)-C(4)	122.6(3)
I(6)#2-Pb(3)-I(4)	101.779(9)	N(1)-C(12)-C(11)	117.2(3)
I(6)-Pb(3)-I(4)#2	101.780(9)	C(4)-C(12)-C(11)	120.2(3)
I(6)-Pb(3)-I(4)	78.221(9)	N(3)-C(13)-C(14)	123.6(4)
I(6)#2-Pb(3)-I(6)	180.0	C(15)-C(14)-C(13)	118.7(3)

Pb(2)-I(1)-Pb(1)	74.720(9)	C(14)-C(15)-C(16)	119.2(4)
Pb(1)-I(2)-Pb(2)	76.402(8)	C(15)-C(16)-C(17)	122.3(4)
Pb(1)-I(3)-Pb(2)	75.896(9)	C(24)-C(16)-C(15)	118.0(4)
Pb(2)-I(4)-Pb(3)	76.913(9)	C(24)-C(16)-C(17)	119.7(3)
Pb(2)-I(5)-Pb(3)	78.958(8)	C(18)-C(17)-C(16)	120.1(4)
Pb(3)-I(6)-Pb(2)	75.435(9)	C(17)-C(18)-C(19)	121.8(4)
Mn(2)-I(7)-Mn(1)	83.65(3)	C(20)-C(19)-C(18)	122.9(4)
Mn(1)-I(8)-Mn(2)	82.09(3)	C(23)-C(19)-C(18)	119.6(3)
I(7)-Mn(1)-I(8)	96.86(3)	C(23)-C(19)-C(20)	117.5(4)
Cl(2)-Mn(1)-Cl(1)	82.36(5)	C(21)-C(20)-C(19)	119.2(4)
N(5)-Mn(1)-I(7)	93.22(9)	C(20)-C(21)-C(22)	119.7(4)
N(5)-Mn(1)-I(8)	100.17(9)	N(4)-C(22)-C(21)	123.6(4)
N(5)-Mn(1)-Cl(1)	98.01(9)	N(4)-C(23)-C(19)	123.1(3)
N(5)-Mn(1)-Cl(2)	102.68(9)	N(4)-C(23)-C(24)	118.1(3)
N(5)-Mn(1)-N(6)	74.65(12)	C(19)-C(23)-C(24)	118.9(3)
N(5)-Mn(1)-N(7)	90.66(12)	N(3)-C(24)-C(16)	122.7(3)
N(5)-Mn(1)-N(8)	157.90(10)	N(3)-C(24)-C(23)	117.5(3)
N(6)-Mn(1)-I(7)	167.86(9)	C(16)-C(24)-C(23)	119.8(3)
N(6)-Mn(1)-I(8)	85.15(8)	N(5)-C(25)-C(26)	122.6(4)
N(6)-Mn(1)-Cl(1)	169.56(8)	C(27)-C(26)-C(25)	120.3(4)
N(6)-Mn(1)-Cl(2)	91.92(9)	C(26)-C(27)-C(28)	119.3(4)
N(6)-Mn(1)-N(7)	98.35(10)	C(27)-C(28)-C(29)	123.0(4)
N(7)-Mn(1)-I(7)	81.88(8)	C(36)-C(28)-C(27)	117.5(3)
N(7)-Mn(1)-I(8)	169.15(8)	C(36)-C(28)-C(29)	119.5(4)
N(7)-Mn(1)-Cl(1)	89.02(9)	C(30)-C(29)-C(28)	121.1(4)
N(7)-Mn(1)-Cl(2)	164.97(8)	C(29)-C(30)-C(31)	120.8(4)
N(8)-Mn(1)-I(7)	99.47(8)	C(32)-C(31)-C(30)	122.1(4)
N(8)-Mn(1)-I(8)	96.21(9)	C(32)-C(31)-C(35)	117.9(4)

N(8)-Mn(1)-Cl(1)	97.02(9)	C(35)-C(31)-C(30)	119.9(4)
N(8)-Mn(1)-Cl(2)	95.30(9)	C(33)-C(32)-C(31)	119.6(4)
N(8)-Mn(1)-N(6)	92.18(11)	C(32)-C(33)-C(34)	118.9(4)
N(8)-Mn(1)-N(7)	73.48(12)	N(6)-C(34)-C(33)	122.8(4)
I(7)-Mn(2)-I(8)	96.83(3)	N(6)-C(35)-C(31)	122.7(4)
Cl(1)-Mn(2)-Cl(2)	82.73(5)	N(6)-C(35)-C(36)	118.4(3)
N(1)-Mn(2)-I(7)	168.84(9)	C(31)-C(35)-C(36)	118.9(3)
N(1)-Mn(2)-I(8)	81.02(8)	N(5)-C(36)-C(28)	122.3(4)
N(1)-Mn(2)-Cl(1)	162.84(10)	N(5)-C(36)-C(35)	117.9(3)
N(1)-Mn(2)-Cl(2)	87.70(9)	C(28)-C(36)-C(35)	119.8(3)
N(2)-Mn(2)-I(7)	96.63(9)	N(7)-C(37)-C(38)	124.0(4)
N(2)-Mn(2)-I(8)	98.69(9)	C(39)-C(38)-C(37)	118.9(5)
N(2)-Mn(2)-Cl(1)	94.13(9)	C(38)-C(39)-C(40)	120.0(4)
N(2)-Mn(2)-Cl(2)	97.67(9)	C(39)-C(40)-C(41)	124.3(4)
N(2)-Mn(2)-N(1)	73.01(11)	C(48)-C(40)-C(39)	116.7(4)
N(2)-Mn(2)-N(3)	92.26(11)	C(48)-C(40)-C(41)	119.0(4)
N(3)-Mn(2)-I(7)	85.73(8)	C(42)-C(41)-C(40)	122.3(4)
N(3)-Mn(2)-I(8)	168.36(8)	C(41)-C(42)-C(43)	120.9(4)
N(3)-Mn(2)-Cl(1)	93.13(9)	C(44)-C(43)-C(42)	124.1(4)
N(3)-Mn(2)-Cl(2)	169.48(8)	C(44)-C(43)-C(47)	117.2(4)
N(3)-Mn(2)-N(1)	98.57(11)	C(47)-C(43)-C(42)	118.7(4)
N(4)-Mn(2)-I(7)	101.53(9)	C(45)-C(44)-C(43)	120.8(4)
N(4)-Mn(2)-I(8)	94.40(8)	C(44)-C(45)-C(46)	117.8(5)
N(4)-Mn(2)-Cl(1)	105.77(9)	N(8)-C(46)-C(45)	124.6(4)
N(4)-Mn(2)-Cl(2)	97.78(8)	N(8)-C(47)-C(43)	122.5(4)
N(4)-Mn(2)-N(1)	89.57(12)	N(8)-C(47)-C(48)	116.9(3)
N(4)-Mn(2)-N(2)	156.14(10)	C(43)-C(47)-C(48)	120.6(4)
N(4)-Mn(2)-N(3)	73.96(11)	N(7)-C(48)-C(40)	123.2(4)

Mn(2)-Cl(1)-Mn(1)	97.25(7)	N(7)-C(48)-C(47)	118.5(3)
Mn(1)-Cl(2)-Mn(2)	95.17(6)	C(40)-C(48)-C(47)	118.3(4)
C(1)-N(1)-Mn(2)	127.7(3)		

Symmetry transformations used to generate equivalent atoms: #1 -x-1, -y, -z+2; #2 -x-2, -y+1, -z+2.

Reference:

1. W. M. Wendlandt, H. G. Hecht, *Reflectance Spectroscopy*. Interscience: New York, 1966.

2. (a) M. D. Segall, P. J. D. Lindan, M. J. Probert, C. J. Pickard, P. J. Hasnip, S. J. Clark, M. C. Payne, *J. Phys.: Condens. Matter,* **2002,** *14*, 2717-2744; (b) V. Milman, B. Winkler, J. A. White, C. J. Pickard, M. C. Payne, E. V. Akhmatskaya, R. H. Nobes, *Int. J. Quantum Chem.,* **2000,** *77*, 895-910.

3. D. R. Hamann, M. Schluter, C. Chiang, *Phys. Rev. Lett.,* **1979,** *43*, 1494-1497.

4. Agilent, *CrysAlisPro*. Version 1.171.35.21 ed.; Agilent Technologies Corp.: California, America.

5. Siemens, *SHELXTL Version 5 Reference manual*. Siemens Energy & Automaion Inc.: Madision,WI, 1994.

6. (a) Q. Hou, F. Q. Bai, M. J. Jia, J. Jin, J. H. Yu, J. Q. Xu, *CrystEngComm,* **2012,** *14*, 4000-4007; (b) M. A. Tershansy, A. M. Goforth, L. Peterson, M. C. Burns, M. D. Smith, H. C. zur Loye, *Solid State Sci.,* **2007,** *9*, 895-906; (c) G. V. Prakash, K. Pradeesh, R. Ratnani, K. Saraswat, M. E. Light, J. J. Baumberg, *J. Phys. D: Appl. Phys.,* **2009,** *42*, 185405; (d) H. Krautscheid, C. Lode, F. Vielsack, H. Vollmer, *J. Chem. Soc., Dalton Trans.,* **2001,** 1099-1104.

7. (a) B. Saparov, D. B. Mitzi, *Chem. Rev.,* **2016,** *116*, 4558-4596; (b) L. Pedesseau, D. Sapori, B. Traore, R. Robles, H. H. Fang, M. A. Loi, H. H. Tsai, W. Y. Nie, J. C. Blancon, A. Neukirch, S. Tretiak, A. D. Mohite, C. Katan, J. Even, M. Kepenekian, *ACS Nano,* **2016,** *10*, 9776-9786; (c) C. Q. Ma, D. Shen, M. F. Lo, C. S. Lee, *Angew. Chem., Int. Ed.,* **2018,** *57*, 9941-9944; (d) T. Jeon, S. J. Kim, J. Yoon, J. Byun, H. R. Hong, T. W. Lee, J. S. Kim, B. Shin, S. O. Kim, *Adv. Energy Mater.,* **2017,** *7*, 1602596.